Self-organization in precipitation reactions far from the equilibrium

Elias Nakouzi and Oliver Steinbock*

Far from the thermodynamic equilibrium, many precipitation reactions create complex product structures with fascinating features caused by their unusual origins. Unlike the dissipative patterns in other self-organizing reactions, these features can be permanent, suggesting potential applications in materials science and engineering. We review four distinct classes of precipitation reactions, describe similarities and differences, and discuss related challenges for theoretical studies. These classes are hollow micro- and macrotubes in chemical gardens, polycrystalline silica carbonate aggregates (biomorphs), Liesegang bands, and propagating precipitation-dissolution fronts. In many cases, these systems show intricate structural hierarchies that span from the nanometer scale into the macroscopic world. We summarize recent experimental progress that often involves growth under tightly regulated conditions by means of wet stamping, holographic heating, and controlled electric, magnetic, or pH perturbations. In this research field, progress requires mechanistic insights that cannot be derived from experiments alone. We discuss how mesoscopic aspects of the product structures can be modeled by reaction-transport equations and suggest important targets for future studies that should also include materials features at the nanoscale.

INTRODUCTION

The rational design of systems that create complex materials and functional devices by externally controlled self-organization holds great promise for modern materials science (1). Progress toward this goal requires an understanding of how materials synthesis is affected by transport processes, steep concentration gradients, and other factors that arise from reaction conditions far from the equilibrium. A plethora of examples, providing inspiration and proof of concept, is found among biological systems that use nonconventional bottom-up strategies to produce remarkable materials. For instance, biominerals, such as bones and tooth enamel, are strikingly different from—and in many ways superior to—the crystal structures formed near the thermodynamic equilibrium by direct mixing of the reactants (2). Instead of bulk crystals or individual nanoparticles with tailored but limited properties, these natural materials typically consist of thousands of nanosized building blocks that assemble into functionality-enhancing hierarchies of structures. The most important initial challenge for the production of similar, nonbiological materials is the selection of suitable model systems that can serve as stepping stones toward technologically relevant applications; however, even for simple systems, progress can be expected to be slow, unless theoretical research develops mechanistic models. Because of the complexity of the involved processes and the wide range of relevant length scales, these models also present unique computational challenges that need to be met to arrive at a paradigm shift from current synthetic approaches to controlled, "lifelike" nonequilibrium methods.

The coupling of nonlinear reactions and transport processes is ideally suited to create and maintain steep concentration gradients that can serve as positional and directional guides for the synthesis and/or assembly of materials. They allow the relay of information over macroscopic length scales and, hence, potentially bridge the gap between the molecular world and the realm of microstructures and devices. Thus it

is not surprising that reaction-transport phenomena are ubiquitous in nature and represent the de facto mode of operation in living systems. Alan Turing, a pioneer of biological pattern formation, recognized that a "system of chemical substances…reacting together and diffusing through a tissue is adequate to account for the main phenomena of morphogenesis" (3). Specifically, Turing formulated the possible chemical basis for stationary spatial patterns that are now being discussed as the source patterns on mollusk shells (4), zebra stripes and leopard spots (5), and even cortical folding (6, 7). In addition, reaction-diffusion–type equations have been used to model neural signals (8), cardiac arrhythmias (9, 10), uterine contractions (11), and a broad range of other dynamical processes (12). Similar examples from chemistry include pattern formation in the autocatalytic Belousov-Zhabotinsky reaction (13, 14), the CO oxidation on platinum catalysts (15), gas discharge systems (16), corrosion processes (17, 18), electrochemical deposition (19, 20), and frontal polymerization (21). Many of these systems create self-propagating reaction zones that, in two or three dimensions, organize more complex patterns ranging from labyrinthine shapes (22) to spiral waves and, in some cases, create unique materials in their wake. Even more ambitious studies have demonstrated the formation of self-assembling fluidic machines (23, 24), biomimetic organic-inorganic hybrids (25, 26), and chemoresponsive gel materials (27, 28).

In this comparative review, we discuss four distinct classes of precipitation systems that couple reaction kinetics and transport to produce unexpected, nonequilibrium materials: (i) chemical gardens, which are centimeter-sized, hollow tubes that are formed by the rapid precipitation of metal (hydr)oxides and typically amorphous silica; (ii) silica-carbonate biomorphs, which are complex microstructures that consist of highly aligned, crystalline nanorods; (iii) Liesegang patterns, which self-organize periodic precipitation bands by the simple counter-diffusion of two complementary electrolytes; and (iv) propagating reaction pulses that produce dynamic patterns by balancing precipitation and redissolution processes. Despite many chemical and dynamical similarities between these systems, there exist equally important differences that we highlight in Table 1. For example, the products of these reaction

Department of Chemistry and Biochemistry, Florida State University, Tallahassee, FL 32306–4390, USA.
*Corresponding author. Email: steinbock@chem.fsu.edu

systems show varying levels of complexity, with characteristic length scales in the order of nanometers in the case of biomorphs to centimeters for the hollow tubes. Their rates of formation range from seconds to hours and even days, and are controlled by fluid flow and spontaneous compartmentalization (chemical gardens), diffusive transport and Ostwald ripening (periodic precipitation), and reaction-driven assembly (biomorphs). Currently, the level of theoretical modeling of these processes ranges from well developed, as in the case of periodic precipitation, to nonexistent for silica-carbonate biomorphs.

Over the past years, research on these four system classes has provided direct contributions to a broad range of disciplines, including geochemistry, astrobiology, and the fundamentals of crystallization. For example, chemical gardens are a synthetic analog of the chimney structures in deep-sea hydrothermal vents, which are thought to be a likely locale for the onset of prebiotic chemistry and the origin of life (29, 30). Silica-carbonate biomorphs have demonstrated that purely inorganic processes can form lifelike microstructures, thus suggesting that morphology alone cannot be used to validate the biogenicity of fossils (31). Similarly, periodic precipitation explains layered intrusions and striations that occur in certain rock formations (32). By comparison, the impact of this research on materials synthesis has remained relatively small so far, which, in our opinion, is not due to fundamental limitations but rather reflect limited effort. However, several recent advances have opened new and exciting horizons: periodic precipitation has been scaled down to nano- and micropatterns with a remarkable degree of control (33), chemical gardens have been functionalized with quantum dots (34) and constrained to quasi–two-dimensional layers (35), and biomorphs have been rationally designed into complex biomimetic structures (36). These and other results provide important stepping stones toward one of the ultimate goals of "Materials by Design": programming chemical reactions in space and time to spontaneously assemble the desired complex products.

HOLLOW TUBES

Chemical gardens are the most iconic and oldest example of pattern formation through precipitation reactions (37–39). These lifelike landscapes consist of hollow, inorganic tubes with diameters of around 1 mm and lengths of several centimeters. They form spontaneously when a solid salt particle is placed into an aqueous solution containing anions such as silicate, borate, carbonate, phosphate, sulfide, or even hydroxide (Fig. 1, A to D) (40, 41). In the classic example of reactions with silicates, the thin tube wall consists of metal (hydr)oxide and an outer layer of amorphous silica that can also be absent (42). The growth commences with the dissolution of metal salt, which gives rise to the formation of a colloidal metal (hydr)oxide membrane around the dissolving seed particle and the subsequent breach of this membrane due to an osmotically driven flow of water. From the breach site, buoyant salt water rises up and rapidly reacts at the liquid interface with the alkaline silicate solution to form a new precipitate that effectively compartmentalizes the two reaction partners. These processes can give rise to open structures that form around a buoyant jet or closed structures that expand through subsequent self-healing breaches and/or a more steady reaction-mediated expansion of the membrane area.

The chemistry of the chemical garden phenomenon is extremely diverse, and hollow tubes have been studied not only for the reactants listed above but also in polyoxometalate systems (43–45), solid metals undergoing corrosion (46, 47), organic reactions (48), and even under natural sea ice that forms downward-growing conduits of ice called brinicles (49). Also of great interest are the chimney-like precipitate structures near hydrothermal vents at the ocean floor (for example, black smokers and off-axis alkaline vents) where, near volcanically active regions (50–53), hot, mineral-rich water surges into cold sea water (Fig. 1E). Theories that these natural chimneys were the birthplace of life on our planet (29, 30, 54–56) have been suggested. Advantages of this specific origin-of-life hypothesis include (i) confinement of reactive

Table 1. Qualitative comparison of the four classes of precipitation reactions discussed in this review. The classical pattern size refers to the length scales one encounters in the typical experiment, but deviations usually exist in specialized cases (see text).

	Chemical gardens	Biomorphs	Liesegang bands	Precipitation pulses
Pattern-forming precipitation reactions	Yes	Yes	Yes	Yes
Thermodynamic driving force	Interfacial reactions	Global supersaturation	Local supersaturation	Local supersaturation and redissolution
Typical reactants	Very diverse	$BaCl_2$, $SrCl_2$, or $CaCl_2$ and Na_2SiO_3, CO_2/Na_2CO_3	Very diverse	$AlCl_3$ or $ZnCl_2$ and NaOH, $HgCl_2$, and NaI
Dominant macroshape	Hollow tubes	Sheets and helices	Bands of crystals	Planar fronts and spirals
Classical pattern size	1 mm (tube radius), 1 dm (tube length)	1 μm (sheet height), 20 μm (helix width)	1 mm (band spacing)	0.1 mm (pulse width), 1 mm (spiral pitch)
Typical initial condition	Crystal seed or injection	Homogeneous solution or influx of gas	Solution over gel in tube	Solution over gel in Petri dish
Dominant nanostructure	Amorphous/nanocrystals	Polycrystalline and aligned nanorods	Colloids to macrocrystals	Colloids to macrocrystals
Present in nature	Hydrothermal vents and brinicles	Possibly (pseudofossils)	Layered intrusions and agates	Unknown
Mathematical models	Only for specific features	No	Advanced	Advanced
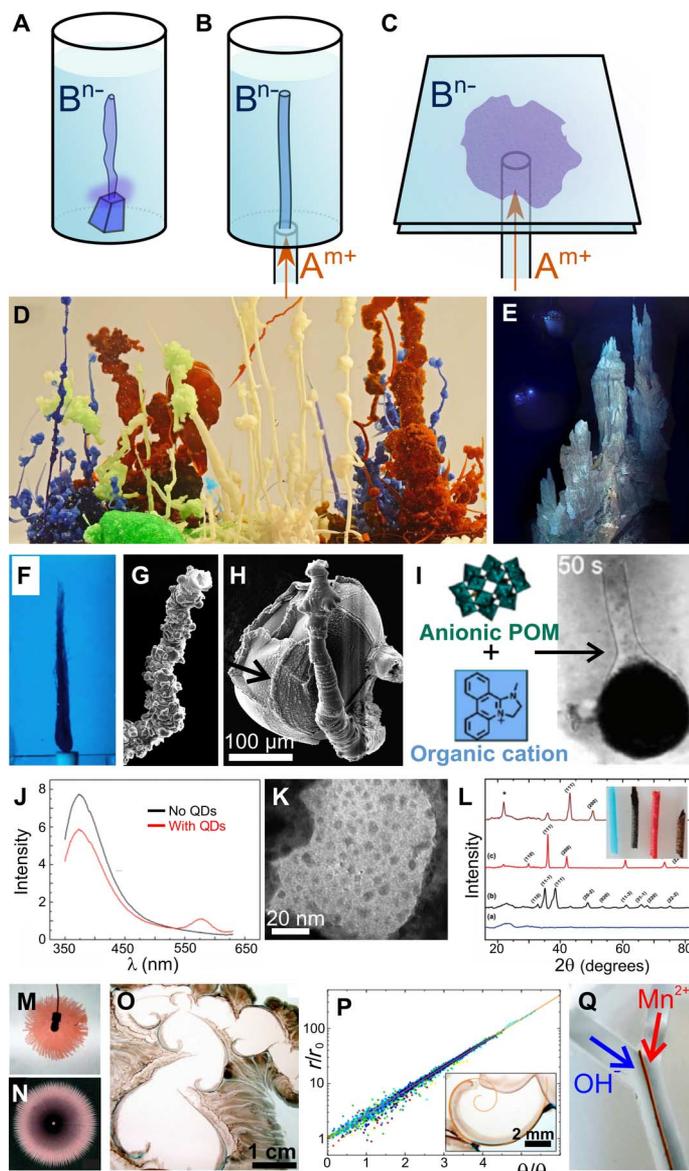
Fig. 1. Chemical gardens. (**A** to **C**) Schematics of experiments using (A) a seed crystal, (B) solution injection, and (C) a spatially confined system. (**D**) Typical example of chemical gardens. (**E**) Hydrothermal vent at Lost City [adapted with permission from Kelly *et al.* (*51*)]. (**F**) $Cu(OH)_2$ tube formed by solution injection method [adapted with permission from Baker *et al.* (*64*)]. (**G** and **H**) Microtube from reactant-loaded polymer beads that develop rim structures (arrow). (**I**) Microtubes from a polyoxometalate (POM) precipitation reaction [adapted with permission from Cooper *et al.* (*45*)]. (**J** and **K**) Emission spectrum (J) and transmission electron microscopy (K) image of quantum dot (QD)–functionalized zinc oxide/hydroxide tubes [adapted with permission from Makki *et al.* (*34*)]. (**L**) Postsynthetic processing of copper hydroxide tube to produce various copper-based materials [adapted with permission from Uechi *et al.* (*72*)]. (**M** to **O**) Thin-layered chemical gardens of (M and O) cobalt hydroxide [adapted with permission from Batista *et al.* (*73*)] and (N) cobalt oxalate [adapted with permission from Roszol *et al.* (*75*)]. (**P**) Scaling law reveals logarithmic spiral shapes [adapted with permission from Haudin *et al.* (*35*)]. (**Q**) Precipitate membranes formed by double injection in microfluidic device [adapted with permission from Batista and Steinbock (*83*)].

solutions to micro- and macropores without lipids, (ii) the presence of geochemical catalysts including iron and nickel (hydr)oxides and sulfides, (iii) a long-lived source of free energy in the form of pH and other gradients, and (iv) a steady flow of reactants including hydrogen, methane, and carbon monoxide.

Many modern experiments on tube formation in chemical gardens replace the solid reactant seed with a corresponding solution that is injected at constant flow rates or, as recently demonstrated, at constant driving pressures (*57*–*65*). The obvious advantages of this method are that only single tubes are formed and that the overall reproducibility is greatly improved (Fig. 1F). Furthermore, the concentration, viscosity, and density of the two reactant solutions are (at least initially) known. Using this method, several distinct growth regimes were identified, all of which strongly depend on the buoyancy of the injected solution. Also, a rigorous fluid dynamic equation was derived to describe the radius of open tubes templated by jets (*66*). More recently, a simple power law dependence $v \propto Q^{3/2}$ between the vertical growth rate v and the used flow rate Q was reported (*67*). In another version of this experiment, the outer solution is steadily delivered to a large pellet of the seed salt (*68*). These experiments can produce tubes of very large diameter that allow measurement of interior ion concentrations using inserted electrodes.

One of the many interesting aspects of the inorganic structures for materials science is that the newly formed wall is self-healing in ways that are very poorly understood to date. This feature is most striking for closed tube structures that can grow because of steady stretching of the membrane or rhythmic ruptures followed by an immediate capping of the breach site. Regardless of the specific chemistry, the initial membrane can grow by a reaction-transport–mediated process that not only stretches the membrane but also simultaneously thickens it. As the membrane ages, this feature is partially lost, and one can observe the formation of cracks in the now brittle material. However, these cracks directly expose the two reactive liquids to each other, and thus cause the rapid formation of a new material that sometimes creates a polygonal network of scar-like rims.

An experiment in which these processes are very pronounced involves a polymer bead–based modification of the classical chemical garden experiment (*69*). Here, the metal salt is loaded into the beads with diameters in the range of 10 to 100 μm, which are then exposed to the silicate solution. Some of the beads simply surround themselves with a precipitate shell, whereas others also form outwardly extending hollow microtubes (Fig. 1, G and H). The shells typically show the aforementioned crack patterns as elevated rim structures (Fig. 1H, arrow) and can be extracted from the product solution for further use or analysis. The tubes have inner diameters of down to 10 μm and lengths of up to a millimeter because their growth is limited by the finite reactant reservoir in the salt-saturated bead. In terms of the bead radius R and the loading concentration c, the bead-tube border follows a curve $cR \approx \text{const}$ with tubes occurring for high values of c or R. This interesting finding can be understood quantitatively if one considers the amount of reactant n in the bead ($n \propto R^3$), the amount consumed during shell formation ($n \propto R^2$), and the fact that tube formation occurs after the shell growth is essentially complete.

Microtubes also form in the polyoxometalate reactions studied by Cronin *et al.* (Fig. 1I) (*43*–*45*). The growth direction of these microstructures can be controlled by holographic heating, which induces fluid flow near the growth zone at the open end of the tube (*43*–*45*, *70*, *71*). Furthermore, reconnection events can be provoked, which effectively create

junction points between different tube segments. Notice that the tube acts as its own reactant-delivering conduit in all of these experiments, regardless of whether the self-organized tube connects to a bead, crystal, or solution reservoir. Similar directional changes were noted if the tube was exposed to externally applied electric fields (44), although some doubts exist as to whether those effects were actually caused by electric fields and not by temperature gradients and fluid flow. The growth of tubes can also be influenced by external magnetic fields, as demonstrated by Stone and Goldstein and Uechi *et al.* (47, 72). All of these experiments provide an ideal testing ground for modeling efforts based on reaction-transport equations.

The existence of microtubes with high aspect ratios and the possibility of controlling their growth direction suggest that it should be possible to construct complex three-dimensional tube networks that could be useful as the main conduit structure for microfluidic applications. In addition, one can envision the use of the precipitate tubes as special components in conventional (glass- or elastomer-based) microfluidic devices where they locally alter electrophoretic flow or provide catalytic functionalities as well as sensory readout points. In this context, we note that the tube wall can be readily modified both during and after formation. For example, Makki *et al.* reported the trapping of CdSe/ZnS quantum dots during tube growth (34). After synthesis, the trapped particles were chemically accessible to solutes in the surrounding solution, as demonstrated by experiments that quenched the photoluminescence of the dots with Cu(II) ions (Fig. 1, J and K). Batista *et al.* showed that larger structures such as polymer beads and biological cells can also be incorporated into the tubes (73). In all of these experiments, the guest units were simply dispersed within the injected reactant solution. The main material of the growing tube wall can also be layered by means of specific injection sequences. In 2011, Roszol and Steinbock demonstrated this procedure for the example of macrotubes that consisted of layers of silica, copper hydroxide, and zinc hydroxide (74). The latter hydroxides can be typically transformed into the corresponding oxides by simple heating (Fig. 1L). These experiments exposed the tubes to a temperature of nearly 900°C, with only minimal breakage of the structures. In the case of silica-supported $Zn(OH)_2$, the structures transform to photocatalytically active ZnO, which also shows the expected photoluminescence of this material. In the case of blue $Cu(OH)_2$, the material transforms sequentially to black CuO and red Cu_2O and can even be further processed to silica-supported Cu(0), all with only minimal loss of the tubes' integrity (75).

More recent variations of the chemical garden experiment have created precipitation structures beyond the simple hollow tube geometry. For example, Haudin *et al.* demonstrated the rapid formation of complex morphologies by the injection of one of the reacting species into a thin solution layer of its complementary ion (35, 76, 77). This setup is similar to Hele-Shaw cells that have been used to study viscous fingering in fluid dynamics. Another related experiment is the injection of a significantly more concentrated solution that is relatively dense, which also results in the formation of thin-layered precipitates (78–81). The complexity of precipitation landscapes observed in the cobalt-silicate (35) and cobalt-oxalate (78) systems is demonstrated in Fig. 1 (M to O). Some of the obtained patterns have been characterized as logarithmic spirals (Fig. 1P). Another variant of this experiment involves precipitation at the air-fluid interface when a buoyant metal ion solution is pumped to the surface of a silicate solution (82). Furthermore, one-dimensional membranes similar in composition to chemical gardens have been grown in microfluidic devices (83). These precipitate walls

form at the interface between two flowing solutions and can be tailored to any macroscopic geometry (Fig. 1Q). Further experiments will test their catalytic properties and, in particular, their potential role as analogs of geochemical precipitation membranes that possibly drove the synthesis of complex organics on early Earth (84).

SILICA-CARBONATE BIOMORPHS

Silica-carbonate biomorphs present another exciting model system for the emergence of complex microstructures from simple precipitation reactions (36, 85–87). In the most common example, biomorphs are formed by the coprecipitation of alkaline earth metal carbonates and amorphous silica in a highly alkaline medium (Fig. 2, A to C). These purely inorganic reactions self-organize structures with lifelike shapes such as cardioid leaves (Fig. 2D), helical filaments (Fig. 2, E and F), wavy curtains (Fig. 2G), and conical funnels (Fig. 2, H and I) (31, 88–90). The defining hallmark of silica-carbonate biomorphs is their smoothly curved, noneuhedral shapes that are not restricted to the typical crystallographic symmetries. At the nanoscale, these structures arrange thousands of crystalline nanorods into highly ordered assemblies that resemble natural biominerals (Fig. 2J). However, whereas biomineralization relies on scores of proteins to control crystal size, habit, and polymorph selection (2), biomorphs assemble spontaneously and without the assistance of any organic additives.

Despite their structural complexity, biomorphs are synthesized using simple experimental procedures (87, 91): specifically the solution-gel (Fig. 2A), gas diffusion (Fig. 2B), or single-phase methods (Fig. 2C). In the first approach, an aqueous solution of alkaline earth metal ions and predissolved carbon dioxide is added on top of a silica gel layer. The diffusion of the M^{2+} and CO_3^{2-} ions into the gel prompts the coprecipitation of silica and metal carbonate. Because of the gradients in pH and reactant concentrations, the obtained morphologies vary markedly along the depth of the gel layer (92, 93). Later studies showed that similar biomorphs can be synthesized using the gas diffusion method, in which a solution of silicate and metal ions is exposed to the influx of atmospheric carbon dioxide (94–96). Alternatively, tetraethoxysilane can be used as a reliable source of silicate ions (97). Most recently, biomorphs have been grown using a conceptually even simpler approach known as the single-phase method. In the latter case, all of the precursor ions (CO_3^{2-}, M^{2+}, and SiO_3^{2-}) are present in the reaction solution and stored under inert nitrogen gas to prevent the influx of carbon dioxide (91). This method minimizes the decrease in solution pH that occurs in other setups and, hence, allows the routine growth of biomorphs up to several millimeters under stable chemical conditions.

The remarkable variety of structures that emerge in the biomorph precipitation system is shown in Fig. 2 (D to I). The three most common biomorphs are the cardioid sheet, the double helix, and the single helix or "worm-like" morphology (87). García-Ruiz *et al.* suggested a qualitative growth mechanism that connects these principal biomorph shapes (85). In the early growth stages, a barium carbonate single crystal undergoes successive branching induced by the adsorption of silicate ions on the growing crystal lattice (Fig. 2K). Eventually, this branching results in the formation of a globule through the rod-fractal-dumbbell pathway (98). The growth mode then changes abruptly and a thin sheet of crystalline nanorods begins to extend from the globule (Fig. 2L). At some point during this expansion, the biomorph sheet curls upward, which causes a local arrest in its growth. This curl then propagates along
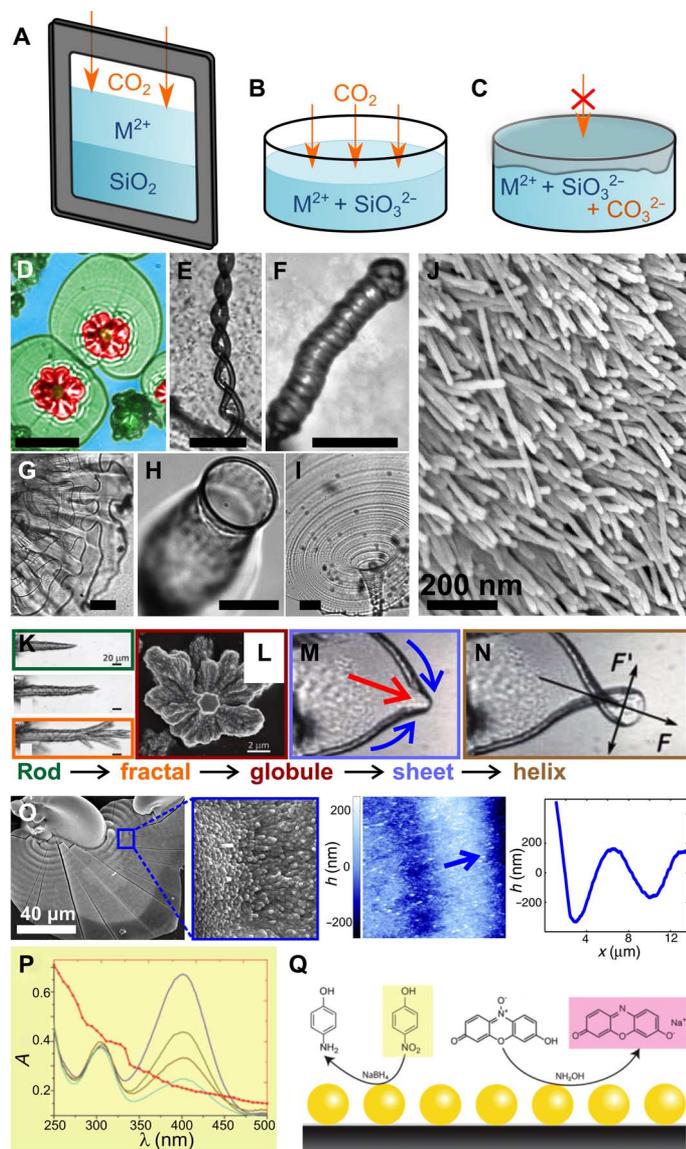
Fig. 2. Silica-carbonate biomorphs. (**A** to **C**) Schematics of experimental setups: (A) gel-solution, (B) gas diffusion, and (C) single-phase methods. (**D** to **I**) Optical micrographs of biomorphs showing (D) leaf (false coloring), (E) double helix, (F) single helix or worm, (G) wavy curtain, (H) micro-urn, and (I) funnel structures. (J) Coaligned nanorods that constitute the biomorph structures [D to J; adapted with permission from Nakouzi et al. (91)]. (**K** to **N**) Stages of biomorph growth from (K) rod, to (L) globule, (M) sheet, and, eventually, (N) double helix [adapted with permission from García-Ruiz et al. (85)]. (**O**) Periodic height variations along the biomorph sheet surface due to nanorod alignment waves observed in SEM and AFM [adapted with permission from Nakouzi et al. (105)]. (**P** and **Q**) Catalytic reactions with gold-functionalized biomorphs: (P) UV-visible spectra showing reduction of *p*-nitrophenol by NaBH₄ and (Q) scheme of surface-catalyzed reactions [adapted with permission from Opel et al. (117)]. A, absorbance.

the sheet perimeter and eventually results in the distinctive cardioidal shape (Fig. 2M). When these two curls meet at the sheet edge, they intertwine to form a single or double helix, depending on their relative size and handedness (Fig. 2N). In some cases, the thin sheets can completely curl away from the growth substrate and expand freely to form coral-like shapes or wavy curtains. Other biomorph structures include hollow microstructures, such as urns or cones, with smoothly varying diameters and remarkably circular cross sections (91). Although these diverse morphologies often coexist in the same crystallization solutions, the reaction conditions can statistically favor the formation of certain structures. For example, helical biomorphs commonly form in the single-phase method at pH <10.8, whereas the wavy sheets are the dominant morphology at higher pH values (91). Other factors such as polymeric or protein additives (99, 100) and the inclusion of other metal carbonates that compete in the coprecipitation process (101, 102) can significantly influence biomorph growth.

Although most studies have focused on the mesoscale dynamics of biomorph growth, some attempts have been made toward delineating the underlying chemical mechanism. One hypothesis by García-Ruiz et al. suggests the occurrence of local pH oscillations that drive the coprecipitation of the metal carbonate and amorphous silica (85, 103). In this scenario, the crystallization of barium carbonate nanorods induces a pH decrease in the vicinity of the growing crystals. This local change in the chemical environment promotes the precipitation of amorphous silica, which, in turn, increases the pH again and results in the further formation of barium carbonate nanocrystals. Accordingly, biomorph growth is only possible within a narrow range of initial conditions that exploit this autocatalytic feedback to drive the coprecipitation. To date, there has not been direct experimental evidence for this mechanism. A recent study using a pH-sensitive fluorescent dye showed that the biomorph-solution interface maintains a significantly lower pH value compared to the bulk solution (104). However, there were no observations of temporal pH oscillations that would validate the hypothesized mechanism. Another study highlighted the occurrence of "topographic" oscillations of the biomorph sheets (Fig. 2O) (105). These features form immediately in the wake of the crystallization front, suggesting that they are caused by the local chemical environment, but their relevance to the pH oscillations model has been challenged. For example, they are not accompanied by compositional oscillations that would suggest the alternating crystallization of silica and barium carbonate (105). Moreover, the spatial wavelength of these oscillations is largely independent from the reactant concentrations, which is a rather surprising observation for a presumed reaction-diffusion–type process.

Another exciting aspect of silica-carbonate biomorphs is their morphological similarity to the fossilized remains of primitive life forms. The most interesting examples are the oldest known Archean putative fossils found in the Warrawoona Chert of Western Australia. These microstructures had been described as filamentous cyanobacteria that date back 3.5 billion years (106, 107), but more recent studies cast doubts on their biogenic origins (108, 109). The presumed fossils were preserved in silica cherts that show an abundance of barite and carbonate minerals. This geochemical setting is possibly conducive to biomorph precipitation and suggests that the Warrawoona microstructures might have formed by abiotic mineralization. Accordingly, biomorphs provide a powerful proof of concept that morphology cannot be considered as conclusive evidence for the biogenicity of primitive fossils on Earth and elsewhere. However, it is worth noting that field observations of naturally occurring biomorphs have not yet been recorded. The most

relevant present-day terrestrial environment that might support bio-morph growth is the Ney spring in California (*110*, *111*). These natural spring waters show an unusually high pH of approximately 11.6 and a silicate ion concentration greater than 4000 ppm (*110*). Future studies using these waters and similar natural environments will demonstrate the role of silica-carbonate biomorphs in understanding the overlap between geochemistry, paleontology, and the detection of primitive life on Earth and other planets.

In addition to being a truly a unique class of precipitation structures, silica-carbonate biomorphs are a challenging example of self-assembly across different length scales. At the moment, a rigorous understanding of biomorph growth is clearly lacking—from the nucleation of their nanoscale building blocks to their arrangement into highly ordered, hier-archical architectures. For example, it remains unclear whether the carbonate nanorods are instantaneously cemented into position during growth or coalign after their crystallization. In the latter case, it will be important to determine the range, magnitude, and nature of the forces that drive their assembly and to map the free energy landscape of this process. Some of these problems require the direct observation of bio-morph growth with temporal and nanoscale spatial resolution using in situ techniques such as liquid phase transmission electron microscopy (*112*, *113*). Another open question is the chemical composition of these complex structures at the nanoscale. Although it is well established that biomorphs consist of predominantly alkaline earth metal carbonates and amorphous silica, the spatial distribution of these components has remained a mystery (*114*). One suggestion is that the carbonate nano-rods are supported by an amorphous silica matrix similar to organic templates in natural biominerals. Alternatively, the silica species might simply be incorporated within the carbonate nanorods. Solving these open questions will have a significant impact on the current debate re-garding the fundamentals of crystallization and nonclassical pathways of nucleation and crystal growth (*115*, *116*). For materials synthesis, silica-carbonate biomorphs suggest an avenue for producing functional, hier-archical structures with potentially interesting optical, catalytic, and biomedical applications (*117*, *118*). For instance, Opel *et al.* reported the functionalization of biomorphs by postsynthetic silanization fol-lowed by the immobilization of gold nanoparticles at the biomorph sur-face (*117*). The gold-functionalized structures were then used as platforms for catalyzing organic reactions such as the reduction of *p*-nitrophenol by $NaBH_4$ (Fig. 2, P and Q).

PERIODIC PRECIPITATION

Standard chemistry textbooks and common intuition suggest that at macroscopic lengthscales, precipitation reactions tend to form disordered and overall unremarkable products. However, the delicate coupling between precipitation kinetics and reactant transport can pro-duce ordered patterns and self-organize complex structures. One of the prime examples is periodic precipitation, which has remained a fascinating phenomenon since its discovery by Raphael Edward Liesegang in the late 19th century (*119*, *120*). Liesegang patterns are produced in a simple experimental setup: an aqueous solution of an "outer" electrolyte is layered onto a gel containing its complementary "in-ner" electrolyte (Fig. 3, A to C). Specifically, the diffusion of the outer electrolyte into the reaction medium induces the formation of regu-larly spaced precipitate aggregates. These patterns are periodic bands in one spatial dimension, rings in two dimensions, or shells in three

dimensions (*121*, *122*). Other structures that emerge at different re-action conditions include helicoidal precipitates, fractal patterns, and regular crystals (*123*–*126*). Because of the simplicity of the underlying chemical principles, Liesegang patterns have been observed for a broad range of systems involving metals (such as Ag^+, Pb^{2+}, Fe^{2+}, Zn^{2+}, Ca^{2+}, and Mg^{2+}) and their precipitate counter-anions (I^-, F^-, S^{2-}, OH^-, CrO_4^{2-}, $Cr_2O_7^{2-}$, and SO_4^{2-}), even extending beyond the laboratory to geo-chemical and mineralogical environments (*127*, *128*).

The spatiotemporal arrangement of Liesegang patterns is highly reg-ular and follows simple empirical laws. For example, the relative location of the precipitate bands is described by the Jabłczyński law: $x_{n+1}/x_n = 1 + p$, where x_n is the distance of the *n*th band from the solution-gel interface, and $1 + p$ is a system-specific spacing coefficient (*129*). In most cases, the value of p is positive, which corresponds to an increasing interband dis-tance. However, some systems such as silver iodide and lead chromate also show decreasing interband distance, commonly referred to as revert spacing (*130*). The transition between direct and revert spacing behav-ior is not well understood but has been ascribed to the adsorption of the outer electrolyte on the already formed precipitation bands. Moreover, the Matalon-Packter law describes the dependence of p on the initial ion concentrations according to $p = f(b_0) + g(b_0)/a_0$, where a_0 and b_0 denote the outer and inner electrolyte concentrations, respectively (*131*). In ad-dition to these general observations for interband spacing, a simple power law describes the width (w) of the precipitation bands, which typ-ically increases at distances farther from the gel-solution interface according to $w \propto x_n^\alpha$, $\alpha > 0$. Finally, the fourth empirical law, which was discovered by Morse and Pierce, captures the temporal dynamics of Liesegang band formation as $x_n = \sqrt{\delta t_n}$, where t_n is the time at which the *n*th band begins to precipitate (*132*). Notice that the scaling co-efficient δ is analogous to a diffusion constant, which is not a surprising result in the limit of fast reaction kinetics and slow diffusive transport. These simple empirical laws hold for a broad range of Liesegang systems and reaction conditions.

Since the discovery of Liesegang bands, many attempts have been undertaken to explain these chemical patterns using theoretical models. In 1897, Wilhelm Ostwald suggested that periodic precipitation is driv-en by a repeating cycle of supersaturation, nucleation, and depletion (*1*). Specifically, the diffusion of the outer electrolyte into the reaction me-dium increases the local ion concentrations beyond a threshold super-saturation value. As a result, microcrystals begin to nucleate and grow, creating a distinct precipitation band that eventually lowers the ion con-centrations in its close vicinity. Accordingly, the precipitate does not grow homogeneously throughout the reaction medium; instead, the dif-fusion of reactant ions creates supersaturation conditions at a farther location, leading to the formation of another precipitation band. This so-called "prenucleation" model and its more complex variations (*1*) have been used to simulate the qualitative Liesegang features and the experi-mentally observed scaling laws. A second class of "postnucleation" models describes the competitive growth of small crystallites. In this scenario, the precipitating salts form a sol of colloidal particles that spread homogeneously within the gel. Subsequently, Ostwald ripening occurs, by which the relatively larger crystals grow at the expense of more soluble, smaller particles. The precipitate then self-organizes into characteristic Liesegang bands that are rich in crystal aggregates and gaps which contain almost no crystals. The postnucleation model can also predict the formation of secondary striations that sometimes emerge between the primary Liesegang bands (*133*). Several studies have also in-vestigated the effect of extrinsic factors such as temperature gradients

(134), applied electric fields (135, 136), or exposure to microwave radiation (137) on the rhythmicity of Liesegang patterns.

In addition to being an important case of chemical self-organization, Liesegang banding is directly relevant to geochemical pattern formation (32, 138, 139). For example, "layered intrusions" in igneous rocks (solidified magma and lava) show precipitation bands of alternating chemical composition such as chromite ($FeCr_2O_4$) striations in predominantly olivine (Mg_2SiO_4) and silicate minerals (140) or pyroxene doublet bands in a plagioclase matrix (different forms of silicate minerals) (141). These have been successfully simulated using various reaction-transport models that follow Liesegang-type mechanisms but also account for system-specific factors such as advective transport, heat conduction, and latent heat release. Other examples from sedimentary rocks include precipitate rings formed in iron oxide minerals, octocalcic phosphate, and ruin marble (32). A common feature in many of these systems is the infiltration of an ion-rich liquid through the fractures of already existing rocks. This mechanism has been tested experimentally by pumping a concentrated sulfuric acid solution through a thin tube into a sample of ferruginous limestone (142). The acid dissolves the calcite ($CaCO_3$) mineral and induces the precipitation of millimeter-scale gypsum bands ($CaSO_4$). We emphasize that these results do not suggest that all stratification patterns in nature are directly related to Liesegang banding or similar types of geochemical self-organization. Extrinsic factors such as bacterial activity or annual climate variations can also template patterns that are deceivingly similar to Liesegang structures. However, the tools of nonlinear chemical dynamics and self-organization no doubt provide an excellent platform for understanding this diverse range of geochemical and mineralogical systems.

In the classic Liesegang experiment, the diffusion of the reacting ions is disrupted by hydrodynamic backflow near the gel-solution interface. Accordingly, the first regular bands form beyond an initial zone that is typically in the order of a few millimeters (Fig. 3D). Grzybowski et al. developed a technique known as wet stamping that prevents this fluid disturbance and allows the scaling of Liesegang rings to dimensions of micrometers and even of nanometers (33, 143). In this setup, a disc-like agarose "stamp" is loaded with the outer electrolyte and placed in contact with a thin layer of gelatin containing the inner electrolyte. The interdiffusion of the two species induces the precipitation of Liesegang microbands that consist of crystalline nanoparticles. The size of the particles within each band is relatively monodisperse and generally increases for bands at further distances from the electrolyte source (144, 145). Moreover, the agarose stamps can be sculpted into arbitrary geometries with microscale features to control the formation of complex Liesegang geometries (Fig. 3, E to J). For example, the spacing coefficient p is regulated by the gel thickness (H), the distance between the stamp features (L), and the size of these features (d). This degree of control allows the fabrication of two-dimensional patterns with potential applications in diffractive optics (146, 147). In three spatial dimensions, the periodic precipitation can assemble nano- and microscopic wrinkles of increasing heights (Fig. 3K) (148). The wet stamping technique provides a powerful tool for synthesizing highly ordered structures from simple reaction-diffusion processes.

An emerging frontier in this field is the design of reaction-diffusion systems in which the reaction partners are not small, precipitate-forming ions but rather colloidal or polymeric building blocks. Some promising first steps have already been taken in this direction. For example, Lagzi et al. used oppositely charged nanoparticles (Au or Ag) as the outer and inner "electrolytes" in a Liesegang-type setup (Fig. 3L) (149). The nanoparticles self-organize into periodic bands with the characteristic spacing properties of Liesegang patterns. However, the formation of these bands is not related to a conventional solubility product but a cluster threshold and the constraint of electroneutrality. In a similar experiment, Nabika et al. investigated the diffusion of silver ions into a gelatin matrix loaded with a reducing agent such as citrate (150). This reaction-diffusion experiment resulted in the synthesis of silver nanoparticles that are spatially distributed into classic Liesegang bands. Another interesting application is the gelation of certain polysaccharides called κ-carrageenan that can be induced by a sufficiently high concentration of alkali metal ions. Recent studies show that the diffusion of potassium ions into an aqueous solution of κ-carrageenan produces a gel with spatially nonhomogeneous properties that match
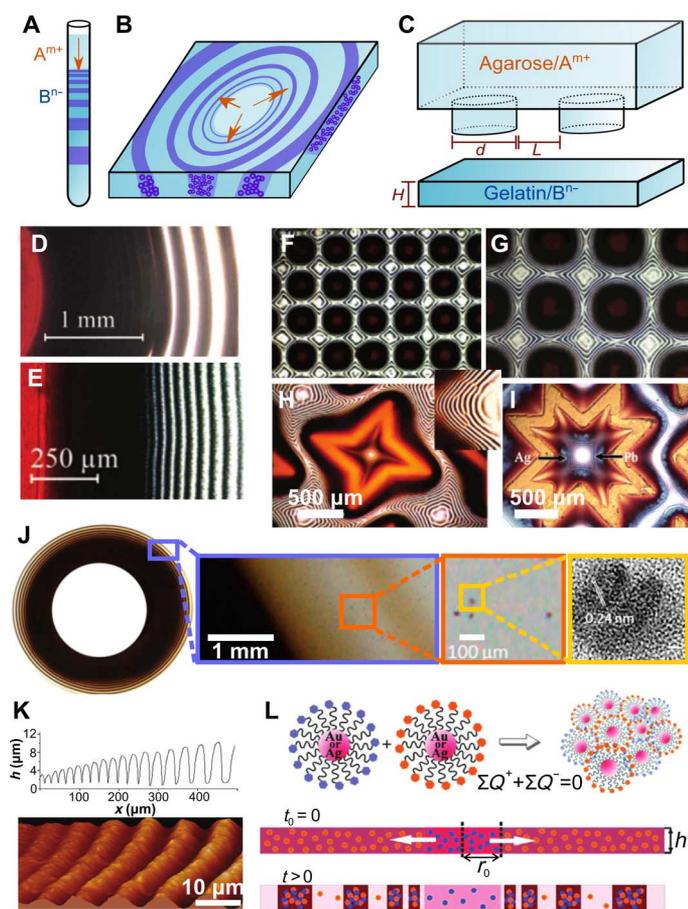

Fig. 3. Periodic precipitation. (**A** to **C**) Schematics of experiments in (A) one-dimensional tubes, (B) two-dimensional slabs, and (C) using the wet stamping technique. (**D** and **E**) Comparison of Liesegang patterns in the (D) traditional and (E) wet stamping setups. (**F** to **J**) Assortment of precipitation micropatterns in (F and G) $Ag^+/Cr_2O_7^{2-}$, (H and I) $Ag^+,Pb^{2+}/Cr_2O_7^{2-}$ [D to I; adapted with permission from Bensemann et al. (33)], and (J) Ag^+/citrate systems [adapted with permission from Nabika et al. (150)]. (**K**) Controlled precipitation of $Ag_2Cr_2O_7$ microwrinkles with linearly increasing height [adapted with permission from Walliser et al. (145)]. (**L**) Periodic precipitation setup for nanoparticle aggregation [adapted with permission from Lagzi et al. (149)].

a Liesegang pattern (*151, 152*). These exciting results suggest a novel paradigm for materials production under which the synthesis is not only designed to form a product with a specific molecular composition but also programmed to create a defined spatial distribution (*153–155*).

DYNAMIC PRECIPITATION-DISSOLUTION PATTERNS

So far, we have only discussed precipitation patterns that form stationary structures in the wake of a propagating reaction front. However, interesting dynamics occur if the precipitate formation is coupled to a second reaction that causes redissolution (Fig. 4, A to C). For example, in the classic Liesegang setup, this condition is satisfied if hydroxide and chromium(III) ions are used as the outer and inner electrolytes, respectively (*156, 157*). For these reactants, one observes a propagating band of chromium(III) hydroxide precipitation (reaction 1)

$$Cr^{3+} + 3OH^- \rightarrow Cr(OH)_3 \downarrow \tag{1}$$

$$Cr(OH)_3 + OH^- \rightarrow [Cr(OH)_4]^- \tag{2}$$
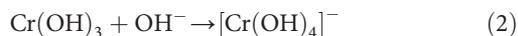
followed by redissolution and the formation of the soluble $[Cr(OH)_4]^-$ complex due to diffusive influx of surplus hydroxide ions (reaction 2). The resulting traveling precipitate band is of finite, macroscopic width and is easily detectable. The leading boundary layer of the band corresponds to the $Cr^{3+}/Cr(OH)_3$ interface, while the receding layer is the $Cr(OH)_3/[Cr(OH)_4]^-$ interface. The propagation speed of the band decreases with increasing distance (x) from the gel-solution boundary according to $x^2 \propto t$, and thus suggests a diffusion-controlled process. Moreover, the width of the band is almost constant for a given set of reaction conditions, but decreases with increasing Cr^{3+} ion concentration. The band propagation ceases after a few days, and the system then self-organizes a classic Liesegang pattern. The crossover from a traveling precipitation band to a periodic pattern suggests mechanistic commonalities between these different behaviors. Furthermore, similar precipitation-dissolution dynamics have been reported for other reaction couples such as $Co(OH)_2/[Co(NH_3)_6]^{2+}$, $HgI_2/[HgI_4]^{2-}$, and $Al(OH)_3/[Al(OH)_4]^-$ (*158–161*). Additional observations in these systems include the occurrence of dynamic Liesegang patterns, temporal chaos in the number of precipitation bands, and a nontrivial spatial distribution of these bands (Fig. 4D) (*162–164*).

The behavior of precipitation-dissolution bands becomes significantly more complex when the system is extended from the quasi–one-dimensional test tube geometry to two spatial dimensions. One such experimental setup involves the preparation of a gel medium of the inner electrolyte (Al^{3+}) and cutting a disc-like hole, which is then filled with a solution of the outer electrolyte (OH^-) (*165–167*). As the hydroxide ions invade the gel, a precipitate ring begins to propagate from the central reservoir outward (Fig. 4E). The width of this pulse can be controlled by the concentrations of the reactant ions. For certain initial conditions, the traveling precipitate eventually stops and a second (and third) precipitate ring forms at the inner interface to propagate in the opposite direction (Fig. 4E) (*168*). Alternatively, the hydroxide solution in the central reservoir can be replaced by an acid solution after the emergence of the first pulse (*165*). In this scenario, a second front

emerges from the center and reprecipitates the aluminum hydroxide complex, predominantly leaving Al^{3+} ions in its wake. Using this method, the amphoteric properties of $Al(OH)_3$ allow the precise control of the spatial distribution of the precipitate and the other reacting species. Volford *et al.* showed that the shape and width of the precipitate pulse can also be purposefully distorted or lowered to the microscale (*165*). For example, the hydroxide reservoir can be surrounded by peripheral acid reservoirs, which create a spatially defined pH field in the reaction medium (Fig. 4F) (*169*). In this setup, a radially symmetric precipitate begins to emerge from the central reservoir but soon becomes distorted because of the flux of H^+ ions. The shape and location of the precipitate pattern can be controlled by the geometry of the reservoirs and the ion concentrations. Because the pH field is controlled by diffusion, the patterns are very smooth and symmetric, which suggests interesting applications for micropatterning.

By slightly modifying the experimental method, complex dynamic patterns beyond simple propagating bands have also been obtained. For example, when hydroxide solution is layered over an Al^{3+}-loaded gel (Fig. 4A), aluminum hydroxide precipitate begins to propagate downward with a leading edge of abrupt precipitation and a trailing edge of
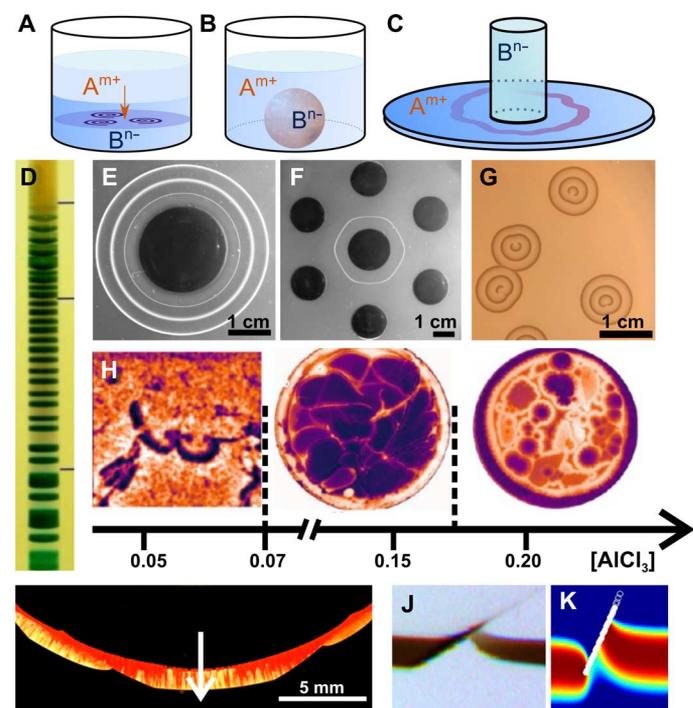
Fig. 4. Dynamic precipitation-dissolution patterns. (**A** to **C**) Schematics of various experimental setups. (**D**) Irregular band spacing in the $Co(OH)_2/Ni(OH)_2$ precipitation-redissolution system [adapted with permission from Msharrafieh and Sultan (*163*)]. (**E** to **G**) Precipitation pulses (E), distorted fronts (F) [adapted with permission from Volford *et al.* (*165*)], and spiral patterns (G) in $Al(OH)_3$ system [adapted with permission from Volford *et al.* (*166*)]. (**H**) Pattern selection in the aluminum hydroxide system as a function of reactant ion concentration [adapted with permission from Dúzs *et al.* (*171*)]. (**I**) Cusp-like front in HgI_2 system [adapted with permission from Ayass and Al-Ghoul (*173*)]. (**J**) Diagonal feature in a downward propagating front observed experimentally (J) and in simulations (K) [adapted with permission from Tinsley *et al.* (*170*)].

redissolution. Although these dynamics follow our earlier description, surprising structures emerge within the precipitate band (170). As illustrated in Fig. 4G, circular target patterns form spontaneously and expand horizontally in the plane of the downwardly propagating precipitate band. If one of the wave fronts in these "cutout patterns" is perturbed or mechanically broken, it organizes into a pair of counter-rotating spiral waves (Fig. 4G). Moreover, collisions between these waves cause mutual annihilation. Further experiments were conducted in a flow reactor that continuously supplies the reactant ions and thus maintains nonequilibrium chemical conditions (171). In this system, a pattern-free precipitate layer forms after a short induction period but then swiftly develops patterns similar to those shown in Fig. 4H. These domain-like structures dissolve and reprecipitate multiple times, showing interesting oscillatory dynamics. Other observations include flower-like precipitation patterns consisting of circular rings with segmented radial fingers. Note that the precipitation-dissolution dynamics discussed here are clearly analogous to chemical waves in a homogeneous excitable medium such as the Belousov-Zhabotinsky reaction (13).

Self-organization of target and spiral patterns is a robust phenomenon that occurs in multiple precipitation systems including zinc hydroxide and mercuric iodide (172). The latter example is particularly interesting because it adds an additional level of complexity because of the polymorph transitions between different HgI_2 crystal structures. Ayass et al. showed that increasing the inner electrolyte concentration (Hg^{2+}) results in the disruption of the circular precipitation fronts and the formation of irregular, sharp cusps (Fig. 4I) (173, 174). By comparison, increasing the outer electrolyte concentration (I^-) has a direct influence on the reaction dynamics, and the system transitions from superdiffusive to subdiffusive transport. The superdiffusive behavior is a particularly surprising observation because it usually requires external forcing of the system. For the spiral wave patterns, the wavelength decreases (increases) with increasing concentration of the inner (outer) electrolyte. Furthermore, the wave velocity decreases with increasing wavelengths, implying an anomalous dispersion relation that is unusual for excitable systems where long wavelengths often ensure full system recovery and fast propagation. These results validate the study of precipitation-complexation systems in the context of excitable medium and hence establish close ties to autocatalytic chemical reactions (13) and cardiac tissue (9). However, one of the main novelties of precipitation reactions is that they form heterogeneous structures through physical phase transitions. This unique feature has allowed the use of propagating reaction fronts for the controlled synthesis of nanoparticles and catalytic microspheres (175–177). These advances open avenues toward the fabrication of dynamic structures that can be coupled to chemical "switches" or used to synthesize otherwise inaccessible nonequilibrium materials.

CHALLENGES FOR COMPUTATIONAL STUDIES

As mentioned earlier, the theoretical understanding of the four classes of precipitation systems differs greatly from essentially undeveloped in the case of biomorphs to well established in the case of Liesegang patterns. The latter example demonstrates the great importance of models and simulations in this overall research area because Liesegang patterns cannot be rationalized by qualitative explanations that are otherwise often successfully used in chemistry. For instance, the specific scaling laws for Liesegang bands are reproduced in simulations

(178, 179) and obviously provided an excellent test for the used models.

Most models in this field have a reaction-diffusion core and critically depend on the initial conditions that vary from spatially homogeneous with a local perturbation representing a nucleation event, to macroscopically separated with a sharp initial interface. A minimal example is the Fisher equation (180) that was originally formulated for the spread of an advantageous gene $u(x,t)$ in the context of population dynamics but also captures some aspects of a solidification or crystallization front

$$\frac{\partial u}{\partial t} = D \frac{\partial^2 u}{\partial x^2} + ku(1-u)$$

Here, the system switches from the steady-state $u = 0$ to a stable steady-state $u = 1$ through a traveling front. In the context of our systems, detailed reaction mechanisms (if available) can be used to replace the simple quadratic function with realistic mass action kinetics and, because multiple reactants are involved, several of these partial differential equations need to be coupled. Furthermore, the actual crystallization process is typically modeled by the use of the Heaviside function $\theta(p\text{-}p^*)$, relating the product concentration (p) to its solubility (p^*).

Although this step in the construction of a model is rather straightforward, numerous complications can arise once additional factors, such as fluid flow and latent heats, are incorporated. Moreover, a simple reaction-diffusion approach is typically limited to macroscopic length scales and fails to model interesting features such as porosity and membrane elasticity (chemical gardens), polymorph selection (most systems), nanoparticle size distributions (Liesegang bands), and nanorod alignment (biomorphs).

The most pressing challenges for computational studies are found for biomorph growth because models are needed to elucidate the mechanisms behind their noneuhedral shapes and accompanying nanorod alignment. In this context, we suggest a possible link between biomorphs and quasi-particles in three-variable nonlinear reaction-diffusion models (181–183). These so-called particles are compact, localized reaction zones that have a characteristic size, shape, and speed. The reaction spots could be equivalent to the crystallization front of sheetlike and, in particular, cylindrical biomorphs. In the presence of additional instabilities, the spot size might oscillate, giving rise to worm-like biomorphs and the interaction of two spots, which is known to create rotation in simulations, could be the origin of helical structures (Fig. 2E). The exploration of this approach would ideally be based on chemically plausible mechanisms but has not been pursued yet. In addition, computational studies could elucidate the important question of whether the aligned nanorods in biomorphs are a passive result of an unrelated process or an active driver of pattern selection in biomorph growth. We suggest that nanorod orientation can be simulated by a director formalism similar to those used for the description of nematic liquid crystals (184) and also of certain biological systems. All of these simulations are computationally expensive because they involve three space dimensions, multiple variables, and steep gradients. Accordingly, the use of advanced computational methods such as adaptive grids and graphics processing unit algorithms (10) will, in many cases, be necessary.

A different set of complications arises in the context of chemical gardens. From a mathematical point of view, tube growth is a free-boundary problem that constitutes its own computational challenges.

For the related phenomenon of dendritic growth, these issues can be addressed by phase-field methods, in which the sharp interface is replaced by a spatially diffuse region of small thickness (*185*). The nature of the interface is further complicated by cross-membrane transport that plays an important role in the thickening of the rigid tube wall. Ding *et al.* recently studied this aspect systematically on the basis of the assumptions that the precipitate is impermeable to the metal ion and that the reaction is almost instantaneous and hence dominated by diffusion (*186*). Their analysis revealed a fluid, dynamically enhanced influx of reactants and quantitatively reproduced the wall thickening in the chemical garden system. The continuous self-healing of soft membranes as well as crack formation in rigid structures followed by rapid sealing are other interesting targets for simulations. Pantaleone *et al.* analyzed tube growth that shows periodic rupturing events and derived equations relating the oscillation period and tube radius to important system parameters (*63*). When compared to experimental data, this analysis yields estimates of the membrane's critical tensile stress and average Young's modulus. Future efforts could possibly combine different existing methods such as those for fast crack propagation (*187*) with those for slow reaction-diffusion processes. Here, however, creative approaches will be needed to bridge not only the time scale gap but, in particular, atomistic features with the macroscopic aspects of the precipitate structures. Disregarding these specific aspects, it would be desirable to at least formulate models that can simulate the basic tube growth process.

Although the description of Liesegang bands and dynamic precipitate patterns is significantly more advanced, a unified theory that captures all the experimental observations does not exist. In this context, some of the successful models have explained the crossover between different dynamic regimes. For instance, Polezhaev and Müller demonstrated the transition from standard Liesegang patterns to helical shapes, aperiodic rings, and other structures using a simple reaction-diffusion model (*178*). Later variations accounted for the complexation of the precipitate in the presence of excess reactant ions and hence predicted the occurrence of precipitation pulses (*167*, *179*, *188*). Another example is the transition from Liesegang rings to stationary spot patterns in the cadmium sulfide/hydroxide system. Dayeh *et al.* explained these dynamics on the basis of a spinodal decomposition model using the nonlinear Cahn-Hilliard equation (*189*). In this description, the formation of metastable colloidal particles is followed by phase separation into the spatially defined patterns. In addition to pattern crossovers, current studies are attempting to capture recently discovered spatiotemporal dynamics such as the propagating fronts with a sharp diagonal feature shown in Fig. 4J. Tinsley *et al.* reproduced this observation numerically by assuming the occurrence of a precursor precipitate phase that forms and redissolves only at the wave front (Fig. 4K) (*170*). On the basis of these promising successes, the next steps will have to aim at extending these models into three spatial dimensions (*190*) and connecting the reaction-diffusion framework with other thermodynamic and crystallographic concepts such as the Ostwald rule of stages and polymorph selection (*191*).

CONCLUSIONS

We discussed four important reaction classes that form diverse nano- to macroscopic structures and morphologies from simple precipitation of colloidal matter and crystals. This diversity raises the question of whether the pattern type can be predicted solely on the basis of the involved

reactants and initial conditions. To date, this question is not easily answered, although certain aspects such as the specificity of biomorphs to alkaline earth metal carbonates appear well established. A firm understanding of these selection rules, and furthermore of possible crossover between the different classes, is important for a wider use of hierarchical self-organization in materials science and engineering. If successful, one would come closer to the vision outlined in a recent Basic Energy Sciences report (*192*): "Imagine the transformation from top-down design of materials and systems with macroscopic building blocks to bottom-up design with nanoscale functional units producing next-generation technological innovation. This is the promise of mesoscale science."

Attainable goals for the near future include the biomimetic nonequilibrium synthesis of materials similar to natural biominerals. Here, inorganic compounds such as silicate or synthetic polymers could take the place of proteins and other biomolecules that, in biology, orchestrate the assembly of nanocrystals. In this context, it is interesting that the nacre of certain mollusk shells actually reveals macroscopic spiral waves that are well known from excitable reaction-diffusion systems (*193*) such as the Belousov-Zhabotinsky reaction and the dynamic precipitation-dissolution patterns discussed here. However, we believe that the true potential of synthetic strategies far from thermodynamic equilibrium lies in the production of meso- and macroscopic shapes that could be used as devices (*1*). These devices will be simple in the beginning and again could mimic biological features such as the venom-filled, fragile spines and spine bundles on certain caterpillars or the branched structure of blood capillaries that in a synthetic setting could deliver reactants deep into three-dimensional cell cultures. All of these efforts will also benefit from the low toxicity of many of the involved materials as well as the low cost of the raw materials. Together, we see a bright future for this research that takes synthesis out of the stirred beaker and exploits its intrinsic self-organization far from the equilibrium.

REFERENCES AND NOTES

1. B. A. Grzybowski, *Chemistry in Motion: Reaction–Diffusion Systems for Micro- and Nanotechnology* (John Wiley and Sons, Chichester, UK, 2009).
2. S. Mann, *Biomineralization: Principles and Concepts in Bioinorganic Materials Chemistry* (Oxford Univ. Press, Oxford, 2001).
3. A. M. Turing, The chemical basis for morphogenesis. *Phil. Trans. R. Soc. B* **237**, 37–72 (1952).
4. A. Gierer, H. Meinhardt, A theory of biological pattern formation. *Kybernetik* **12**, 30–39 (1972).
5. B. Cooper, Turing centenary: The incomputable reality. *Nature* **482**, 465 (2012).
6. J. H. E. Cartwright, Labyrinthine Turing pattern formation in the cerebral cortex. *J. Theor. Biol.* **217**, 97–103 (2002).
7. D. A. Striegel, M. K. Hurdal, Chemically based mathematical model for development of cerebral cortical folding patterns. *PLOS Comput. Biol.* **5**, e1000524 (2009).
8. A. Keane, P. Gong, Propagating waves can explain irregular neural dynamics. *J. Neurosci.* **35**, 1591–1605 (2015).
9. J. M. Davidenko, A. V. Pertsov, R. Salomonsz, W. Baxter, J. Jalife, Stationary and drifting spiral waves of excitation in isolated cardiac muscle. *Nature* **355**, 349–351 (1992).
10. Z. Zhang, O. Steinbock, Local heterogeneities in cardiac systems suppress turbulence by generating multi-armed rotors. *New J. Phys.* **18**, 053018 (2016).
11. E. Pervolaraki, A. V. Holden, Spatiotemporal patterning of uterine excitation patterns in human labour. *Biosystems* **112**, 63–72 (2013).
12. E. Nakouzi, R. E. Goldstein, O. Steinbock, Do dissolving objects converge to a universal shape? *Langmuir* **31**, 4145–4150 (2015).
13. V. Petrov, V. Gáspár, J. Masere, K. Showalter, Controlling chaos in the Belousov—Zhabotinsky reaction. *Nature* **361**, 240–243 (1993).
14. E. Nakouzi, Z. A. Jiménez, V. N. Biktashev, O. Steinbock, Analysis of anchor-size effects on pinned scroll waves and measurement of filament rigidity. *Phys. Rev. E* **89**, 042902 (2014).

15. G. Ertl, Reactions at surfaces: From atoms to complexity (Nobel Lecture). *Angew. Chem. Int. Ed.* **47**, 3524–3535 (2008).

16. Y. A. Astrov, Y. A. Logvin, Formation of clusters of localized states in a gas discharge system via a self-completion scenario. *Phys. Rev. Lett.* **79**, 2983–2986 (1997).

17. J. Christoph, P. Strasser, M. Eiswirth, G. Ertl, Remote triggering of waves in an electrochemical system. *Science* **284**, 291–293 (1999).

18. K. Agladze, O. Steinbock, Waves and vortices of rust on the surface of corroding steel. *J. Phys. Chem. A* **104**, 9816–9819 (2000).

19. V. Fleury, Branched fractal patterns in non-equilibrium electrochemical deposition from oscillatory nucleation and growth. *Nature* **390**, 145–148 (1997).

20. E. Nakouzi, R. Sultan, Fractal structures in two-metal electrodeposition systems I: Pb and Zn. *Chaos* **21**, 043133 (2011).

21. Z. Jiménez, J. A. Pojman, Frontal polymerization with monofunctional and difunctional ionic liquid monomers. *J. Polym. Sci. Pol. Chem.* **45**, 2745–2754 (2007).

22. I. Szalai, P. De Kepper, Turing patterns, spatial bistability, and front instabilities in a reaction–diffusion system. *J. Phys. Chem. A* **108**, 5315–5321 (2004).

23. B. A. Grzybowski, H. A. Stone, G. M. Whitesides, Dynamic self-assembly of magnetized, millimetre-sized objects rotating at a liquid–air interface. *Nature* **405**, 1033–1036 (2000).

24. B. A. Grzybowski, M. Radkowski, C. J. Campbell, J. N. Lee, G. M. Whitesides, Self-assembling fluidic machines. *Appl. Phys. Lett.* **84**, 1798–1800 (2004).

25. L. A. Estroff, A. D. Hamilton, At the interface of organic and inorganic chemistry: Bio-inspired synthesis of composite materials. *Chem. Mater.* **13**, 3227–3235 (2001).

26. H. Li, H. L. Xin, D. A. Muller, L. A. Estroff, Visualizing the 3D internal structure of calcite single crystals grown in agarose hydrogels. *Science* **326**, 1244–1247 (2009).

27. V. V. Yashin, A. C. Balazs, Pattern formation and shape changes in self-oscillating polymer gels. *Science* **314**, 798–801 (2006).

28. X. He, M. Aizenberg, O. Kuksenok, L. D. Zarzar, A. Shastri, A. C. Balazs, J. Aizenberg, Synthetic homeostatic materials with chemo-mechano-chemical self-regulation. *Nature* **487**, 214–218 (2012).

29. L. M. Barge, T. P. Kee, I. J. Doloboff, J. M. P. Hampton, M. Ismail, M. Pourkashanian, J. Zeytounian, M. M. Baum, J. A. Moss, C.-K. Lin, R. D. Kidd, I. Kanik, The fuel cell model of abiogenesis: A new approach to origin-of-life simulations. *Astrobiology* **14**, 254–270 (2014).

30. L. M. Barge, Y. Abedian, M. J. Russell, I. J. Doloboff, J. H. E. Cartwright, R. D. Kidd, I. Kanik, From chemical gardens to fuel cells: Generation of electrical potential and current across self-assembling iron mineral membranes. *Angew. Chem. Int. Ed.* **54**, 8184–8187 (2015).

31. J. M. García-Ruiz, S. T. Hyde, A. M. Carnerup, A. G. Christy, M. J. Van Kranendonk, N. J. Welham, Self-assembled silica-carbonate structures and detection of ancient micro-fossils. *Science* **302**, 1194–1197 (2003).

32. I. L'Heureux, Self-organized rhythmic patterns in geochemical systems. *Philos. Trans. A Math. Phys. Eng. Sci.* **371**, 20120356 (2013).

33. I. T. Bensemann, M. Fialkowski, B. A. Grzybowski, Wet stamping of microscale periodic precipitation patterns. *J. Phys. Chem. B* **109**, 2774–2778 (2005).

34. R. Makki, X. Ji, H. Mattoussi, O. Steinbock, Self-organized tubular structures as platforms for quantum dots. *J. Am. Chem. Soc.* **136**, 6463–6469 (2014).

35. F. Haudin, J. H. E. Cartwright, F. Brau, A. De Wit, Spiral precipitation patterns in confined chemical gardens. *Proc. Natl. Acad. Sci. U.S.A.* **111**, 17363–17367 (2014).

36. W. L. Noorduin, A. Grinthal, L. Mahadevan, J. Aizenberg, Rationally designed complex, hierarchical microarchitectures. *Science* **340**, 832–837 (2013).

37. L. M. Barge, S. S. S. Cardoso, J. H. E. Cartwright, G. J. T. Cooper, L. Cronin, A. De Wit, I. J. Doloboff, B. Escribano, R. E. Goldstein, F. Haudin, D. E. H. Jones, A. L. Mackay, J. Maselko, J. J. Pagano, J. Pantaleone, M. J. Russell, C. I. Sainz-Díaz, O. Steinbock, D. A. Stone, Y. Tanimoto, N. L. Thomas, From chemical gardens to chemobrionics. *Chem. Rev.* **115**, 8652–8703 (2015).

38. R. Makki, L. Roszol, J. J. Pagano, O. Steinbock, Tubular precipitation structures: Materials synthesis under non-equilibrium conditions. *Philos. Trans. A Math. Phys. Eng. Sci.* **370**, 2848–2865 (2012).

39. O. Steinbock, J. H. E. Cartwright, L. M. Barge, The fertile physics of chemical gardens. *Phys. Today* **69**, 44–51 (2016).

40. J. H. E. Cartwright, J. M. García-Ruiz, M. L. Novella, F. Otálora, Formation of chemical gardens. *J. Colloid Interface Sci.* **256**, 351–359 (2002).

41. P. J. Fryfogle, E. J. Nelson, J. J. Pagano, Luminescent tubular precipitation structures from reactant-loaded pellets. *Colloids Surf. A* **485**, 84–90 (2015).

42. J. J. Pagano, S. Thouvenel-Romans, O. Steinbock, Compositional analysis of copper–silica precipitation tubes. *Phys. Chem. Chem. Phys.* **9**, 110–116 (2007).

43. C. Ritchie, G. J. T. Cooper, Y.-F. Song, C. Streb, H. Yin, A. D. C. Parenty, D. A. MacLaren, L. Cronin, Spontaneous assembly and real-time growth of micrometre-scale tubular structures from polyoxometalate-based inorganic solids. *Nat. Chem.* **1**, 47–52 (2009).

44. G. J. T. Cooper, L. Cronin, Real-time direction control of self fabricating polyoxometalate-based microtubes. *J. Am. Chem. Soc.* **131**, 8368–8369 (2009).

45. G. J. T. Cooper, A. G. Boulay, P. J. Kitson, C. Ritchie, C. J. Richmond, J. Thiel, D. Gabb, R. Eadie, D.-L. Long, L. Cronin, Osmotically driven crystal morphogenesis: A general approach to the fabrication of micrometer-scale tubular architectures based on polyoxometalates. *J. Am. Chem. Soc.* **133**, 5947–5954 (2011).

46. D. C. Smith, B. McEnaney, The influence of dissolved oxygen concentration on the corrosion of grey cast iron in water at 50°C. *Corros. Sci.* **19**, 391–394 (1979).

47. D. A. Stone, R. E. Goldstein, Tubular precipitation and redox gradients on a bubbling template. *Proc. Natl. Acad. Sci. U.S.A.* **101**, 11537–11541 (2004).

48. G. Pampalakis, The generation of an organic inverted chemical garden. *Chemistry* **22**, 6779–6782 (2016).

49. J. H. E. Cartwright, B. Escribano, D. L. González, C. I. Sainz-Díaz, I. Tuval, Brinicles as a case of inverse chemical gardens. *Langmuir* **29**, 7655–7660 (2013).

50. A. J. Boyce, M. L. Coleman, M. J. Russell, Formation of fossil hydrothermal chimneys and mounds from Silvermines, Ireland. *Nature* **306**, 545–550 (1983).

51. D. S. Kelley, J. A. Karson, D. K. Blackman, G. L. Früh-Green, D. A. Butterfield, M. D. Lilley, E. J. Olson, M. O. Schrenk, K. K. Roe, G. T. Lebon, P. Rivizzigno; AT3-60 Shipboard Party, An off-axis hydrothermal vent field near the Mid-Atlantic Ridge at 30° N. *Nature* **412**, 145–149 (2001).

52. K. L. Von Damm, Lost City found. *Nature* **412**, 127–128 (2001).

53. W. Martin, J. Baross, D. Kelley, M. J. Russell, Hydrothermal vents and the origin of life. *Nat. Rev. Microbiol.* **6**, 805–814 (2008).

54. L. M. Barge, I. J. Doloboff, L. M. White, G. D. Stucky, M. J. Russell, I. Kanik, Characterization of iron–phosphate–silicate chemical garden structures. *Langmuir* **28**, 3714–3721 (2012).

55. M. J. Russell, W. Nitschke, E. Branscomb, The inevitable journey to being. *Philos. Trans. R. Soc. B Biol. Sci.* **368**, 20120254 (2013).

56. M. J. Russell, L. M. Barge, R. Bhartia, D. Bocanegra, P. J. Bracher, E. Branscomb, R. Kidd, S. McGlynn, D. H. Meier, W. Nitschke, T. Shibuya, S. Vance, L. White, I. Kanik, The drive to life on wet and icy worlds. *Astrobiology* **14**, 308–343 (2014).

57. S. Thouvenel-Romans, O. Steinbock, Oscillatory growth of silica tubes in chemical gardens. *J. Am. Chem. Soc.* **125**, 4338–4341 (2003).

58. J. J. Pagano, T. Bánsági Jr., O. Steinbock, Bubble-templated and flow-controlled synthesis of macroscopic silica tubes supporting zinc oxide nanostructures. *Angew. Chem. Int. Ed.* **47**, 9900–9903 (2008).

59. R. Makki, O. Steinbock, Synthesis of inorganic tubes under actively controlled growth velocities and injection rates. *J. Phys. Chem. C* **115**, 17046–17053 (2011).

60. R. Makki, O. Steinbock, Nonequilibrium synthesis of silica-supported magnetite tubes and mechanical control of their magnetic properties. *J. Am. Chem. Soc.* **134**, 15519–15527 (2012).

61. B. C. Batista, P. Cruz, O. Steinbock, From hydrodynamic plumes to chemical gardens: The concentration-dependent onset of tube formation. *Langmuir* **30**, 9123–9129 (2014).

62. M. R. Bentley, B. C. Batista, O. Steinbock, Pressure controlled chemical gardens. *J. Phys. Chem. A* **120**, 4294–4301 (2016).

63. J. Pantaleone, A. Toth, D. Horvath, L. RoseFigura, W. Morgan, J. Maselko, Pressure oscillations in a chemical garden. *Phys. Rev. E* **79**, 056221 (2009).

64. A. Baker, Á. Tóth, D. Horváth, J. Walkush, A. S. Ali, W. Morgan, Á. Kukovecz, J. J. Pantaleone, J. Maselko, Precipitation pattern formation in the copper(II) oxalate system with gravity flow and axial symmetry. *J. Phys. Chem. A* **113**, 8243–8248 (2009).

65. V. Kaminker, J. Maselko, J. Pantaleone, The dynamics of open precipitation tubes. *J. Chem. Phys.* **140**, 244901 (2014).

66. S. Thouvenel-Romans, W. van Saarloos, O. Steinbock, Silica tubes in chemical gardens: Radius selection and its hydrodynamic origin. *Europhys. Lett.* **67**, 42–48 (2004).

67. B. C. Batista, O. Steinbock, Chemical gardens without silica: The formation of pure metal hydroxide tubes. *Chem. Commun.* **51**, 12962–12965 (2015).

68. F. Glaab, M. Kellermeier, W. Kunz, E. Morallon, J. M. García-Ruiz, Formation and evolution of chemical gradients and potential differences across self-assembling inorganic membranes. *Angew. Chem. Int. Ed.* **124**, 4393–4397 (2012).

69. R. Makki, M. Al-Humiari, S. Dutta, O. Steinbock, Hollow microtubes and shells from reactant-loaded polymer beads. *Angew. Chem. Int. Ed.* **48**, 8752–8756 (2009).

70. A. G. Boulay, G. J. T. Cooper, L. Cronin, Morphogenesis of polyoxometalate cluster-based materials to microtubular network architectures. *Chem. Commun.* **48**, 5088–5090 (2012).

71. L. J. Points, G. J. T. Cooper, A. Dolbecq, P. Mialane, L. Cronin, An all-inorganic polyoxometalate–polyoxocation chemical garden. *Chem. Commun.* **52**, 1911–1914 (2016).

72. I. Uechi, A. Katsuki, L. Dunin-Barkovskiy, Y. Tanimoto, 3D-morphological chirality induction in zinc silicate membrane tube using a high magnetic field. *J. Phys. Chem. B* **108**, 2527–2530 (2004).

73. B. C. Batista, P. Cruz, O. Steinbock, Self-alignment of beads and cell trapping in precipitate tubes. *ChemPhysChem* **16**, 2299–2303 (2015).

74. L. Roszol, O. Steinbock, Controlling the wall thickness and composition of hollow precipitation tubes. *Phys. Chem. Chem. Phys.* **13**, 20100–20103 (2011).

75. L. Roszol, R. Makki, O. Steinbock, Postsynthetic processing of copper hydroxide-silica tubes. *Chem. Commun.* **49**, 5736–5738 (2013).

76. F. Haudin, J. H. E. Cartwright, A. De Wit, Direct and reverse chemical garden patterns grown upon injection in confined geometries. *J. Phys. Chem. C* **119**, 15067–15076 (2015).

77. F. Haudin, V. Brasiliense, J. H. E. Cartwright, F. Brau, A. De Wit, Genericity of confined chemical garden patterns with regard to changes in the reactants. *Phys. Chem. Chem. Phys.* **17**, 12804–12811 (2015).

78. E. Tóth-Szeles, G. Schuszter, Á. Tóth, Z. Kónya, D. Horváth, Flow-driven morphology control in the cobalt–oxalate system. *CrystEngComm* **18**, 2057–2064 (2016).

79. B. Bohner, G. Schuszter, O. Berkesi, D. Horváth, Á. Tóth, Self-organization of calcium oxalate by flow-driven precipitation. *Chem. Commun.* **50**, 4289–4291 (2014).

80. B. Bohner, G. Schuszter, D. Horváth, Á. Tóth, Morphology control by flow-driven self-organizing precipitation. *Chem. Phys. Lett.* **631–632**, 114–117 (2015).

81. B. Bohner, B. Endrődi, D. Horváth, Á. Tóth, Flow-driven pattern formation in the calcium-oxalate system. *J. Chem. Phys.* **144**, 164504 (2016).

82. S. Hussein, J. Maselko, J. T. Pantaleone, Growing a chemical garden at the air–fluid interface. *Langmuir* **32**, 706–711 (2016).

83. B. C. Batista, O. Steinbock, Growing inorganic membranes in microfluidic devices: Chemical gardens reduced to linear walls. *J. Phys. Chem. C* **119**, 27045–27052 (2015).

84. R. Saladino, G. Botta, B. M. Bizzarri, E. Di Mauro, J. M. Garcia Ruiz, A global scale scenario for prebiotic chemistry: Silica-based self-assembled mineral structures and formamide. *Biochemistry* **55**, 2806–2811 (2016).

85. J. M. García-Ruiz, E. Melero-García, S. T. Hyde, Morphogenesis of self-assembled nanocrystalline materials of barium carbonate and silica. *Science* **323**, 362–365 (2009).

86. W. Kunz, M. Kellermeier, Beyond biomineralization. *Science* **323**, 344–345 (2009).

87. M. Kellermeier, H. Cölfen, J. M. García-Ruiz, Silica biomorphs: Complex biomimetic hybrid materials from "sand and chalk." *Eur. J. Inorg. Chem.* **2012**, 5123–5144 (2012).

88. J. M. García Ruiz, A. Carnerup, A. G. Christy, N. J. Welham, S. T. Hyde, Morphology: An ambiguous indicator of biogenicity. *Astrobiology* **2**, 353–369 (2002).

89. T. Terada, S. Yamabi, H. Imai, Formation process of sheets and helical forms consisting of strontium carbonate fibrous crystals with silicate. *J. Cryst. Growth* **253**, 435–444 (2003).

90. S. T. Hyde, A. M. Carnerup, A.-K. Larsson, A. G. Christy, J. M. García-Ruiz, Self-assembly of carbonate-silica colloids: Between living and non-living form. *Physica A* **339**, 24–33 (2004).

91. E. Nakouzi, P. Knoll, O. Steinbock, Biomorph growth in single-phase systems: Expanding the structure spectrum and pH range. *Chem. Commun.* **52**, 2107–2110 (2016).

92. J. M. García-Ruiz, J. L. Amorós, Morphological aspects of some symmetrical crystal aggregates grown by silica gel technique. *J. Cryst. Growth* **55**, 379–383 (1981).

93. E. Melero-García, R. Santisteban-Bailón, J. M. García-Ruiz, Role of bulk pH during witherite biomorph growth in silica gels. *Cryst. Growth Des.* **9**, 4730–4734 (2009).

94. A. E. Voinescu, M. Kellermeier, B. Bartel, A. M. Carnerup, A.-K. Larsson, D. Touraud, W. Kunz, L. Kienle, A. Pfitzner, S. T. Hyde, Inorganic self-organized silica aragonite biomorphic composites. *Cryst. Growth Des.* **8**, 1515–1521 (2008).

95. E. Bittarello, F. R. Massaro, D. Aquilano, The epitaxial role of silica groups in promoting the formation of silica/carbonate biomorphs: A first hypothesis. *J. Cryst. Growth* **312**, 402–412 (2010).

96. J. Eiblmeier, M. Kellermeier, D. Rengstl, J. M. García-Ruiz, W. Kunz, Effect of bulk pH and supersaturation on the growth behavior of silica biomorphs in alkaline solutions. *CrystEngComm* **15**, 43–53 (2012).

97. A. E. Voinescu, M. Kellermeier, A. M. Carnerup, A.-K. Larsson, D. Touraud, S. T. Hyde, W. Kunz, Co-precipitation of silica and alkaline-earth carbonates using TEOS as silica source. *J. Cryst. Growth* **306**, 152–158 (2007).

98. S. Busch, H. Dolhaine, A. DuChesne, S. Heinz, O. Hochrein, F. Laeri, O. Podebrad, U. Vietze, T. Weiland, R. Kniep, Biomimetic morphogenesis of fluorapatite-gelatin composites: Fractal growth, the question of intrinsic electric fields, core/shell assemblies, hollow spheres and reorganization of denatured collagen. *Eur. J. Inorg. Chem.* **1999**, 1643–1653 (1999).

99. M. Kellermeier, F. Glaab, A. M. Carnerup, M. Drechsler, B. Gossler, S. T. Hyde, W. Kunz, Additive-induced morphological tuning of self-assembled silica–barium carbonate crystal aggregates. *J. Cryst. Growth* **311**, 2530–2541 (2009).

100. N. Sánchez-Puig, E. Guerra-Flores, F. López-Sánchez, P. A. Juárez-Espinoza, R. Ruiz-Arellano, R. González-Muñoz, R. Arreguín-Espinosa, A. Moreno, Controlling the morphology of silica–carbonate biomorphs using proteins involved in biomineralization. *J. Mater. Sci.* **47**, 2943–2950 (2012).

101. J. Eiblmeier, S. Dankesreiter, A. Pfitzner, G. Schmalz, W. Kunz, M. Kellermeier, Crystallization of mixed alkaline-earth carbonates in silica solutions at high pH. *Cryst. Growth Des.* **14**, 6177–6188 (2014).

102. H. Imai, T. Terada, S. Yamabi, Self-organized formation of a hierarchical self-similar structure with calcium carbonate. *Chem. Commun.* **9**, 484–485 (2003).

103. M. Wilson, Oscillating chemistry explains complex, self-assembled crystal aggregates. *Phys. Today* **62**, 17–18 (2009).

104. J. Opel, M. Hecht, K. Rurack, J. Eiblmeier, W. Kunz, H. Cölfen, M. Kellermeier, Probing local pH-based precipitation processes in self-assembled silica-carbonate hybrid materials. *Nanoscale* **7**, 17434–17440 (2015).

105. E. Nakouzi, Y. E. Ghoussoub, P. Knoll, O. Steinbock, Biomorph oscillations self-organize micrometer-scale patterns and nanorod alignment waves. *J. Phys. Chem. C* **119**, 15749–15754 (2015).

106. J. W. Schopf, B. M. Packer, Early Archean (3.3-billion to 3.5-billion-year-old) microfossils from Warrawoona Group, Australia. *Science* **237**, 70–73 (1987).

107. J. W. Schopf, Microfossils of the Early Archean Apex chert: New evidence of the antiquity of life. *Science* **260**, 640–646 (1993).

108. M. D. Brasier, O. R. Green, A. P. Jephcoat, A. K. Kleppe, M. J. Van Kranendonk, J. F. Lindsay, A. Steele, N. V. Grassineau, Questioning the evidence for Earth's oldest fossils. *Nature* **416**, 76–81 (2002).

109. B. T. De Gregorio, T. G. Sharp, G. J. Flynn, S. Wirick, R. L. Hervig, Biogenic origin for Earth's oldest putative microfossils. *Geology* **37**, 631–634 (2009).

110. J. H. Feth, S. M. Rogers, C. E. Roberson, Aqua de Ney, California, a spring of unique chemical character. *Geochim. Cosmochim. Acta* **22**, 77–86 (1961).

111. I. Barnes, J. B. Rapp, J. R. O'Neil, R. A. Sheppard, A. J. Gude III, Metamorphic assemblages and the direction of flow of metamorphic fluids in four instances of serpentinization. *Contrib. Mineral. Petr.* **35**, 263–276 (1972).

112. D. Li, M. H. Nielsen, J. R. I. Lee, C. Frandsen, J. F. Banfield, J. J. De Yoreo, Direction-specific interactions control crystal growth by oriented attachment. *Science* **336**, 1014–1018 (2012).

113. C. T. Hendley IV, J. Tao, J. A. M. R. Kunitake, J. J. De Yoreo, L. A. Estroff, Microscopy techniques for investigating the control of organic constituents on biomineralization. *MRS Bull.* **40**, 480–489 (2015).

114. J. Eiblmeier, U. Schürmann, L. Kienle, D. Gebauer, W. Kunz, M. Kellermeier, New insights into the early stages of silica-controlled barium carbonate crystallisation. *Nanoscale* **6**, 14939–14949 (2014).

115. H. Cölfen, M. Antonietti, *Mesocrystals and Nonclassical Crystallization* (John Wiley & Sons, Ltd., Chichester, UK, 2008).

116. J. J. De Yoreo, P. U. P. A. Gilbert, N. A. J. M. Sommerdijk, R. L. Penn, S. Whitelam, D. Joester, H. Zhang, J. D. Rimer, A. Navrotsky, J. F. Banfield, A. F. Wallace, F. M. Michel, F. C. Meldrum, H. Cölfen, P. M. Dove, Crystallization by particle attachment in synthetic, biogenic, and geologic environments. *Science* **349**, aaa6760 (2015).

117. J. Opel, F. P. Wimmer, M. Kellermeier, H. Cölfen, Functionalisation of silica–carbonate biomorphs. *Nanoscale Horiz.* **1**, 144–149 (2016).

118. G. Wang, X. Zhao, M. Möller, S. E. Moya, Interfacial reaction-driven formation of silica carbonate biomorphs with subcellular topographical features and their biological activity. *ACS Appl. Mater. Interfaces* **7**, 23412–23417 (2015).

119. R. E. Liesegang, Ueber einige eigenschaften von gallerten. *Naturw. Wochenschr.* **10**, 353–362 (1896).

120. K. H. Stern, The Liesegang phenomenon. *Chem. Rev.* **54**, 79–99 (1954).

121. L. Badr, Z. Moussa, A. Hariri, R. Sultan, Band, target, and onion patterns in Co(OH)$_2$ Liesegang systems. *Phys. Rev. E* **83**, 016109 (2011).

122. I. Lagzi, Controlling and engineering precipitation patterns. *Langmuir* **28**, 3350–3354 (2012).

123. I. Lagzi, D. Ueyama, Pattern transition between periodic Liesegang pattern and crystal growth regime in reaction–diffusion systems. *Chem. Phys. Lett.* **468**, 188–192 (2009).

124. S. Thomas, I. Lagzi, F. Molnár Jr., Z. Rácz, Probability of the emergence of helical precipitation patterns in the wake of reaction–diffusion fronts. *Phys. Rev. Lett.* **110**, 078303 (2013).

125. S. Thomas, I. Lagzi, F. Molnár Jr., Z. Rácz, Helices in the wake of precipitation fronts. *Phys. Rev. E* **88**, 022141 (2013).

126. S. Thomas, G. Varghese, D. Bárdfalvy, I. Lagzi, Z. Rácz, Helicoidal precipitation patterns in silica and agarose gels. *Chem. Phys. Lett.* **599**, 159–162 (2014).

127. H. Nabika, Liesegang phenomena: Spontaneous pattern formation engineered by chemical reactions. *Curr. Phys. Chem.* **5**, 5–20 (2015).

128. R. F. Sultan, Abdel-Fattah, M. Abdel-Rahman, On dynamic self-organization: Examples from magmatic and other geochemical systems. *Lat. Am. J. Solids Struct.* **10**, 59–73 (2013).

129. M. C. K. Jabłczyński, La formation rythmique des précipités: Les anneaux de Liesegang. *Bull. Soc. Chim. France* **33**, 1592–1603 (1923).

130. T. Karam, H. El-Rassy, R. Sultan, Mechanism of revert spacing in a PbCrO$_4$ Liesegang system. *J. Phys. Chem. A* **115**, 2994–2998 (2011).

131. R. Matalon, A. Packter, The Liesegang phenomenon. I. Sol protection and diffusion. *J. Colloid Sci.* **10**, 46–62 (1955).

132. H. W. Morse, G. W. Pierce, Diffusion and supersaturation in gelatine. *Phys. Rev.* **17**, 129 (1903).

133. S. K. Smoukov, I. Lagzi, B. A. Grzybowski, Independence of primary and secondary structures in periodic precipitation patterns. *J. Phys. Chem. Lett.* **2**, 345–349 (2011).

134. T. Antal, I. Bena, M. Droz, K. Martens, Z. Rácz, Guiding fields for phase separation: Controlling Liesegang patterns. *Phys. Rev. E* **76**, 046203 (2007).

135. R. Sultan, R. Halabieh, Effect of an electric field on propagating Co(OH)$_2$ Liesegang patterns. *Chem. Phys. Lett.* **332**, 331–338 (2000).

136. I. Lagzi, Formation of Liesegang patterns in an electric field. *Phys. Chem. Chem. Phys.* **4**, 1268–1270 (2002).

137. Y. Kanazawa, Y. Asakuma, Precipitation behavior in Liesegang systems under microwave irradiation. *J. Cryst. Process Tech.* **4**, 65–70 (2014).

138. P. Ortoleva, E. Merino, C. Moore, J. Chadam, Geochemical self-organization I: Reaction-transport feedbacks and modeling approach. *Am. J. Sci.* **287**, 979–1007 (1987).

139. P. J. Ortoleva, *Geochemical Self-Organization* (Oxford Univ. Press, Oxford, 1993), vol. 23, 432 pp.

140. A. E. Boudreau, A. R. McBirney, The Skaergaard layered series. Part III. Non-dynamic layering. *J. Petrol.* **38**, 1003–1020 (1997).

141. A. E. Boudreau, Crystal aging and the formation of fine-scale igneous layering. *Mineral. Petrol.* **54**, 55–69 (1995).

142. T. Karam, H. El-Rassy, V. Nasreddine, F. Zaknoun, S. El-Joubeily, A. Z. Eddin, H. Farah, J. Husami, S. Isber, R. Sultan, Pattern formation dynamics in diverse physico-chemical systems. *Chaotic Model. Simul.* **3**, 451–461 (2013).

143. M. Fialkowski, C. J. Campbell, I. T. Bensemann, B. A. Grzybowski, Absorption of water by thin, ionic films of gelatin. *Langmuir* **20**, 3513–3516 (2004).

144. R. M. Walliser, F. Boudoire, E. Orosz, R. Tóth, A. Braun, E. C. Constable, Z. Rácz, I. Lagzi, Growth of nanoparticles and microparticles by controlled reaction–diffusion processes. *Langmuir* **31**, 1828–1834 (2015).

145. R. M. Walliser, R. Tóth, I. Lagzi, D. Mathys, L. Marot, A. Braun, C. E. Housecroft, E. C. Constable, Understanding the formation of aligned, linear arrays of Ag nanoparticles. *RSC Adv.* **6**, 28388–28392 (2016).

146. M. Fiałkowski, A. Bitner, B. A. Grzybowski, Wave optics of Liesegang rings. *Phys. Rev. Lett.* **94**, 018303 (2005).

147. C. J. Campbell, E. Baker, M. Fialkowski, A. Bitner, S. K. Smoukov, B. A. Grzybowski, Self-organization of planar microlenses by periodic precipitation. *J. Appl. Phys.* **97**, 126102 (2005).

148. S. K. Smoukov, A. Bitner, C. J. Campbell, K. Kandere-Grzybowska, B. A. Grzybowski, Nano- and microscopic surface wrinkles of linearly increasing heights prepared by periodic precipitation. *J. Am. Chem. Soc.* **127**, 17803–17807 (2005).

149. I. Lagzi, B. Kowalczyk, B. A. Grzybowski, Liesegang rings engineered from charged nanoparticles. *J. Am. Chem. Soc.* **132**, 58–60 (2010).

150. H. Nabika, M. Sato, K. Unoura, Liesegang patterns engineered by a chemical reaction assisted by complex formation. *Langmuir* **30**, 5047–5051 (2014).

151. T. Narita, M. Tokita, Liesegang pattern formation in κ-carrageenan gel. *Langmuir* **22**, 349–352 (2006).

152. T. Narita, I. Ohnishi, M. Tokita, Y. Oishi, Macroscopic pattern formation of liquid crystal in κ-carrageenan gel. *Colloids Surf. A* **321**, 117–120 (2008).

153. G. M. Whitesides, B. Grzybowski, Self-assembly at all scales. *Science* **295**, 2418–2421 (2002).

154. B. A. Grzybowski, C. J. Campbell, Fabrication using 'programmed' reactions. *Mater. Today* **10**, 38–46 (2007).

155. K. Martens, I. Bena, M. Droz, Z. Rácz, Encoding information into precipitation structures. *J. Stat. Mech. Theory Exp.* **2008**, P12003 (2008).

156. M. Zrinyi, L. Galfi, E. Smidroczki, Z. Racz, F. Horkay, Direct observation of a crossover from heterogeneous traveling wave to Liesegang pattern formation. *J. Phys. Chem.* **95**, 1618–1620 (1991).

157. R. Sultan, S. Panjarian, Propagating fronts in 2D Cr(OH)₃ precipitate systems in gelled media. *Physica D* **157**, 241–250 (2001).

158. R. Sultan, S. Sadek, Patterning trends and chaotic behavior in Co²⁺/NH₄OH Liesegang systems. *J. Phys. Chem.* **100**, 16912–16920 (1996).

159. V. Nasreddine, R. Sultan, Propagating fronts and chaotic dynamics in Co(OH)₂ Liesegang systems. *J. Phys. Chem. A* **103**, 2934–2940 (1999).

160. H. Batlouni, M. Al-Ghoul, Experimental study of the dynamics of front propagation in the Co(OH)₂/NH₄OH Liesegang system using spectrophotometry. *J. Phys. Chem. A* **112**, 8038–8045 (2008).

161. M. M. Ayass, A. Abi Mansour, M. Al-Ghoul, Alternating metastable/stable pattern in the mercuric iodide crystal formation outside the Ostwald rule of stages. *J. Phys. Chem. A* **118**, 7725–7731 (2014).

162. N. Hilal, R. Sultan, Density oscillations in precipitate domains of a propagating Cr(OH)₃ ring. *Chem. Phys. Lett.* **374**, 183–186 (2003).

163. M. Msharrafieh, R. Sultan, Dynamics of a complex diffusion-precipitation-re-dissolution Liesegang pattern. *Chem. Phys. Lett.* **421**, 221–226 (2006).

164. M. Msharrafieh, M. Al-Ghoul, H. Batlouni, R. Sultan, Front propagation in patterned precipitation. 3. Composition variations in two-precipitate stratum dynamics. *J. Phys. Chem. A* **111**, 6967–6976 (2007).

165. A. Volford, F. Izsák, M. Ripszám, I. Lagzi, Systematic front distortion and presence of consecutive fronts in a precipitation system. *J. Phys. Chem. B* **110**, 4535–4537 (2006).

166. A. Volford, F. Izsák, M. Ripszám, I. Lagzi, Pattern formation and self-organization in a simple precipitation system. *Langmuir* **23**, 961–964 (2007).

167. T. Ban, Y. Nagatsu, H. Tokuyama, Propagation properties of the precipitation band in an AlCl₃/NaOH system. *Langmuir* **32**, 604–610 (2016).

168. I. Lagzi, P. Pápai, Z. Rácz, Complex motion of precipitation bands. *Chem. Phys. Lett.* **433**, 286–291 (2007).

169. F. Molnár Jr., L. Roszol, A. Volford, I. Lagzi, Control of precipitation patterns in two-dimensions by pH field. *Chem. Phys. Lett.* **503**, 231–234 (2011).

170. M. R. Tinsley, D. Collison, K. Showalter, Propagating precipitation waves: Experiments and modeling. *J. Phys. Chem. A* **117**, 12719–12725 (2013).

171. B. Dúzs, I. Lagzi, I. Szalai, Propagating fronts and morphological instabilities in a precipitation reaction. *Langmuir* **30**, 5460–5465 (2014).

172. M. M. Ayass, M. Al-Ghoul, I. Lagzi, Chemical waves in heterogeneous media. *J. Phys. Chem. A* **118**, 11678–11682 (2014).

173. M. M. Ayass, M. Al-Ghoul, Superdiffusive cusp-like waves in the mercuric iodide precipitate system and their transition to regular reaction bands. *J. Phys. Chem. A* **118**, 3857–3865 (2014).

174. M. M. Ayass, I. Lagzi, M. Al-Ghoul, Targets, ripples and spirals in a precipitation system with anomalous dispersion. *Phys. Chem. Chem. Phys.* **17**, 19806–19814 (2015).

175. B. Bohner, G. Schuszter, H. Nakanishi, D. Zámbó, A. Deák, D. Horváth, Á. Tóth, I. Lagzi, Self-assembly of charged nanoparticles by an autocatalytic reaction front. *Langmuir* **31**, 12019–12024 (2015).

176. G. A. Al Akhrass, M. Ammar, H. El-Rassy, M. Al-Ghoul, Self-assembled lanthanum hydroxide microspheres within a reaction–diffusion framework: Synthesis, characterization, control and application. *RSC Adv.* **6**, 3433–3439 (2016).

177. D. Saliba, A. Ezzeddine, R. Sougrat, N. M. Khashab, M. Hmadeh, M. Al-Ghoul, Cadmium-aluminum layered double hydroxide microspheres for photocatalytic CO₂ reduction. *ChemSusChem* **9**, 800–805 (2016).

178. A. A. Polezhaev, S. C. Müller, Complexity of precipitation patterns: Comparison of simulation with experiment. *Chaos* **4**, 631–636 (1994).

179. M. Al-Ghoul, R. Sultan, Front propagation in patterned precipitation. 1. Simulation of a migrating Co(OH)₂ Liesegang pattern. *J. Phys. Chem. A* **105**, 8053–8058 (2001).

180. R. A. Fisher, The wave of advantageous genes. *Ann. Hum. Genet.* **7**, 355–369 (1937).

181. C. P. Schenk, M. Or-Guil, M. Bode, H.-G. Purwins, Interacting pulses in three-component reaction–diffusion systems on two-dimensional domains. *Phys. Rev. Lett.* **78**, 3781–3784 (1997).

182. M. Bode, A. W. Liehr, C. P. Schenk, H.-G. Purwins, Interaction of dissipative solitons: Particle-like behaviour of localized structures in a three-component reaction–diffusion system. *Physica D* **161**, 45–66 (2002).

183. H.-G. Purwins, H. U. Bödeker, S. Amiranashvili, Dissipative solitons. *Adv. Phys.* **59**, 485–701 (2010).

184. C. M. Care, D. J. Cleaver, Computer simulation of liquid crystals. *Rep. Prog. Phys.* **68**, 2665–2700 (2005).

185. A. Karma, W.-J. Rappel, Quantitative phase-field modeling of dendritic growth in two and three dimensions. *Phys. Rev. E.* **57**, 4323–4349 (1998).

186. Y. Ding, B. Batista, O. Steinbock, J. H. E. Cartwright, S. S. S. Cardoso, Wavy membranes and the growth rate of a planar chemical garden: Enhanced diffusion and bioenergetics. *Proc. Natl. Acad. Sci. U.S.A* 10.1073/pnas.1607828113 (2016).

187. R. Spatschek, M. Hartmann, E. Brener, H. Müller-Krumbhaar, K. Kassner, Phase field modeling of fast crack propagation. *Phys. Rev. Lett.* **96**, 015502 (2006).

188. F. Izsák, I. Lagzi, Simulation of a crossover from the precipitation wave to moving Liesegang pattern formation. *J. Phys. Chem. A* **109**, 730–733 (2005).

189. M. Dayeh, M. Ammar, M. Al-Ghoul, Transition from rings to spots in a precipitation reaction–diffusion system. *RSC Adv.* **4**, 60034–60038 (2014).

190. M. R. Tinsley, D. Collison, K. Showalter, Three-dimensional modeling of propagating precipitation waves. *Chaos* **25**, 064306 (2015).

191. J. Rahbani, M. Ammar, M. Al-Ghoul, Reaction–diffusion framework: The mechanism of the polymorphic transition of α- to β-cobalt hydroxide. *J. Phys. Chem. A* **117**, 1685–1691 (2013).

192. From quanta to the continuum: Opportunities for mesoscale science. A report for the Basic Energy Sciences Advisory Committee Mesoscale Science Subcommittee (2012).

193. J. H. E. Cartwright, A. Checa, The dynamics of nacre self-assembly. *J. R. Soc. Interface* **4**, 491–504 (2007).

Citation: E. Nakouzi, O. Steinbock, Self-organization in precipitation reactions far from the equilibrium. *Sci. Adv.* **2**, e1601144 (2016).

Science Advances

Self-organization in precipitation reactions far from the equilibrium

Elias Nakouzi and Oliver Steinbock

ARTICLE TOOLS	http://advances.sciencemag.org/content/2/8/e1601144
REFERENCES	This article cites 187 articles, 17 of which you can access for free http://advances.sciencemag.org/content/2/8/e1601144#BIBL
PERMISSIONS	http://www.sciencemag.org/help/reprints-and-permissions

Use of this article is subject to the Terms of Service